Critical Velocity of Vortex Nucleation in Rotating Superfluid ^{3}He-A

V. M. H. Ruutu,[1] J. Kopu,[1] M. Krusius,[1] Ü. Parts,[1] B. Plaçais,[2] E. V. Thuneberg,[1] and W. Xu[1]
[1]*Low Temperature Laboratory, Helsinki University of Technology, HUT, Finland FIN-02015*
[2]*Ecole Normale Supérieure, CNRS URA 1437, 24 rue Lhomond, France F-75231 Paris Cedex 05*
(Received 31 January 1997; revised manuscript received 27 August 1997)

We have measured the critical velocity v_c at which ^{3}He-A in a rotating cylinder becomes unstable against the formation of quantized vortex lines with continuous (singularity-free) core structure. We find that v_c is distributed between a maximum and a minimum limit, which we ascribe to a dependence on the texture of the orbital angular momentun axis $\hat{\mathbf{l}}(\mathbf{r})$ in the cylinder. Slow cooldown through T_c in rotation yields $\hat{\mathbf{l}}(\mathbf{r})$ textures for which the measured v_c's are in good agreement with the calculated instability of the expected $\hat{\mathbf{l}}$ texture. [S0031-9007(97)04804-7]

PACS numbers: 67.57.Fg, 05.70.Fh, 47.32.−y

A first order transition from one phase to another is associated with hysteresis because of the difficulty of nucleating the new phase. Two effects generally reduce the hysteresis. First, thermal or quantum fluctuations cause the new phase to appear before the energy barrier separating the two energy minima vanishes. Second, surfaces, impurities, or other external agents reduce the energy barrier from its intrinsic value. Both phenomena are of crucial importance for the long standing problem of critical velocities and vortex nucleation in superfluids [1], but occur also in more usual phenomena like formation of water droplets or gas bubbles [2]. The purpose of the present work is to study an exceptional case of vortex nucleation where neither fluctuations nor external surfaces should play a role: superfluid ^{3}He-*A*.

In usual superfluids and superconductors the phase slip takes place by creation and motion of zeros in the order parameter [3]. The A phase of ^{3}He is exceptional because the phase slip arises from the motion of the local angular momentum axis $\hat{\mathbf{l}}(\mathbf{r})$. The characteristic length scale of the $\hat{\mathbf{l}}(\mathbf{r})$ texture is macroscopic ~ 10 μm. Therefore all thermal and quantum fluctuations are negligible. Moreover, a rigid boundary condition fixes $\hat{\mathbf{l}}$ perpendicular to the wall of the experimental container. Thus the processes responsible for the critical velocity take place further than 10 μm from the wall, beyond the reach of surface roughness. Instead, the critical velocity v_c for the phase slip depends on the initial $\hat{\mathbf{l}}$ texture. We measure the critical velocity in a rotating cylinder, and find that it may vary within a factor of 6. However, by cooling slowly through the superfluid transition temperature T_c in rotation, the equilibrium texture is created and the measured v_c is in agreement with theoretical calculations.

Anisotropic superflow.—In ordinary superconductors and superfluids, the order parameter has a phase factor $\exp[i\phi(\mathbf{r})]$, and the superfluid velocity is defined as the gradient of the phase, $v_s \propto \nabla\phi$. In ^{3}He-*A* there is an additional phase factor $\exp[i\phi_l(\hat{\mathbf{p}})]$, which depends on the azimuthal angle ϕ_l of the quasiparticle momentum $\mathbf{p}$ with respect to the angular momentum axis $\hat{\mathbf{l}}$. Instead of resolving the two phases separately, one may only define the total phase factor, which can be expressed as $(\hat{\mathbf{m}} + i\hat{\mathbf{n}}) \cdot \hat{\mathbf{p}}$. Here $\hat{\mathbf{l}}$, $\hat{\mathbf{m}}$, and $\hat{\mathbf{n}}$ form an orthonormal triad, which generally depends on the location $\mathbf{r}$. The superfluid velocity is defined as $\mathbf{v}_s = \frac{\hbar}{2m}\sum_k \hat{m}_k \nabla \hat{n}_k$, where the prefactor $\frac{\hbar}{2m}$ equals Planck's constant divided by twice the mass of a ^{3}He atom. This leads to several unusual features. For example, let us take an initially uniform $\hat{\mathbf{l}} \equiv \hat{\mathbf{z}}$, and then tilt the triads so that $\hat{\mathbf{l}}(z)$ forms a helix with an opening angle β and a wave vector q. This leads to a change in $v_{s,z}$ by $\frac{\hbar}{2m}(1 - \cos\beta)q$ without a change in the externally applied phase difference [4]. Thus ^{3}He-*A* can respond to flow by forming an $\hat{\mathbf{l}}$ texture.

The energetics of the current carrying states is contained in the energy functional [5]

$$f = \tfrac{1}{2}\rho_\perp \mathbf{w}^2 + \tfrac{1}{2}(\rho_\parallel - \rho_\perp)(\hat{\mathbf{l}}\cdot\mathbf{w})^2 - C\mathbf{w}\cdot\nabla\times\hat{\mathbf{l}} + C_0(\hat{\mathbf{l}}\cdot\mathbf{w})(\hat{\mathbf{l}}\cdot\nabla\times\hat{\mathbf{l}}) + \tfrac{1}{2}K_s(\nabla\cdot\hat{\mathbf{l}})^2 + \tfrac{1}{2}K_t(\hat{\mathbf{l}}\cdot\nabla\times\hat{\mathbf{l}})^2 + \tfrac{1}{2}K_b|\hat{\mathbf{l}}\times(\nabla\times\hat{\mathbf{l}})|^2 + \tfrac{1}{2}K_5|(\hat{\mathbf{l}}\cdot\nabla)\hat{\mathbf{d}}|^2 + \tfrac{1}{2}K_6[(\hat{\mathbf{l}}\times\nabla)_i\hat{\mathbf{d}}_j)]^2 - \tfrac{1}{2}g_d(\hat{\mathbf{d}}\cdot\hat{\mathbf{l}})^2 + \tfrac{1}{2}g_h(\hat{\mathbf{d}}\cdot\mathbf{H})^2. \quad (1)$$

Here the first two terms describe the anisotropic kinetic energy arising from the counterflow $\mathbf{w} = \mathbf{v}_n - \mathbf{v}_s$. The terms with coefficients C and C_0 contribute to the coupling between $\mathbf{w}$ and inhomogeneous $\hat{\mathbf{l}}(\mathbf{r})$. The five terms with K_i coefficients are gradient energies for $\hat{\mathbf{l}}(\mathbf{r})$ and the spin anisotropy vector $\hat{\mathbf{d}}(\mathbf{r})$. The last two terms arise from the magnetic dipole-dipole interaction, and from the external magnetic field $\mathbf{H}$. In the absence of the dipole coupling, all uniform current carrying states would be unstable [4]. Thus the dipole interaction determines the scale of the critical velocity $v_d = \sqrt{g_d/\rho_\parallel} \sim 1$ mm/s and the length scale $\xi_d = \frac{\hbar}{2m}\sqrt{\rho_\parallel/g_d} \sim 10$ μm. Except for a tiny region near T_c (Fig. 2), v_d is much smaller than is needed to nucleate usual "singular

 0031-9007/97/79(25)/5058(4)$10.00

vortices," such as one encounters in other superfluids [1,6].

Let us drive the current by applying a normal fluid velocity v_n. (This is equivalent to applying a phase difference $\Delta\phi = \frac{2m}{\hbar} v_n L$ between two points a distance L apart.) The flow properties depend on the magnitude and orientation of the magnetic field [7–10]. In general, a uniform state of $\hat{\mathbf{l}}$ is stable for velocities smaller than a first critical velocity v_{c1}. At larger velocities there often is a stable helical texture. The opening angle β of the helix grows continuously from zero with increasing v_n until a second critical velocity v_{c2}. There the helix becomes unstable, and the resulting state depends on how the flow is applied. A continuously sustained dissipative $\hat{\mathbf{l}}$ texture is found when a constant current is driven in a channel. This case has been studied by several groups, most extensively by Bozler and collaborators [11–13]. In our rotating cylinder, a stationary state is restored after one or more vortex lines are formed in a phase slip.

Experiment.—Our sample container is a cylinder which is rotated around its axis with angular velocity Ω. The radius of the cylinder $R \sim 2$ mm is large compared to ξ_d, which means that the normal velocity $\mathbf{v}_n = \mathbf{\Omega} \times \mathbf{r}$ is rectilinear to a good approximation near the cylindrical walls. Therefore, one should see transitions at $\Omega_{c1} = v_{c1}/R$ and $\Omega_{c2} = v_{c2}/R$ corresponding to the critical values of one-dimensional flow. At Ω_{c2} dissipation sets in only temporarily when a vortex line is created. It is driven by the Magnus force into a vortex bundle in the center of the cylinder. As a consequence, the effective driving velocity $v = [\Omega - \Omega_v(N)]R$ is reduced to a subcritical value. Here N is the number of vortices in the bundle $\Omega_v = \kappa N/2\pi R^2$, and κ the circulation of one vortex line. Compared to channel flow, our experiment has high resolution in the measurement of v_{c2}, since the vortices can be counted with a precision of ± 5 lines from the continuous-wave NMR spectrum. Our sensitivity to a helical texture is poor and v_{c1} has not been observed.

Three different sample cylinders have been used, which were fabricated from epoxy or fused quartz with radii $R = 2 - 2.5$ mm, heights $L = 6 - 7$ mm, and different surface roughnesses [6]. No systematic dependence of v_c on the container was found. A small orifice in the center of the bottom plate of the cylinder provides thermal contact via a liquid ^{3}He column to the refrigerator. The NMR field $\mathbf{H}$, which is large compared to the dipole field $H_d = \sqrt{g_d/g_h} \approx 3$ mT, is either axial ($\|\Omega$) or transverse ($\perp\Omega$). The NMR absorption spectrum has two peaks. The frequency shift of the main peak from the Larmor value is used for thermometry. The satellite peak arises from vortex lines [14] and its intensity is proportional to the number of lines N.

Results.—Figure 1 shows two measurements of the amplitude of the satellite peak as a function of Ω. The acceleration is started from rest ($\Omega = N = 0$) at a slow rate ($d\Omega/dt = 10^{-3} - 10^{-5}$ rad/s^2), and the satellite intensity remains zero until a critical velocity $v_c = \Omega_c R$. In the top frame the amplitude starts to increase linearly when Ω_c is exceeded. This means that vortices are nucleated regularly at a v_c that is approximately independent of the number of vortices N in the center of the cylinder.

The acceleration in Fig. 1(a) is stopped at a velocity Ω_{max}. In order to determine N and v_c in this state, the rotation is decelerated until at $\Omega_{min}(N)$ vortices to start to annihilate [16]. The regular parallelogram-like shape of the acceleration/deceleration loop in Fig. 1(a) shows that v_c is approximately constant.

On repeating the measurement, we generally find a considerable spread in v_c. The distribution is evident in Fig. 2, which shows v_c measured for different histories of sample preparation. Because this variation is much larger than seen in one measuring run Fig. 1(a), it has to arise from different metastable states of the system. The only source of metastability in our system is different superfluid states, i.e., different textures of $\hat{\mathbf{l}}$, $\hat{\mathbf{m}}$, $\hat{\mathbf{n}}$, and $\hat{\mathbf{d}}$. Additional evidence for the textural origin of the spread is discussed below.

In Fig. 1(b) the response to acceleration is a sudden jump in the signal, which corresponds to a burst of $\Delta N \approx 90$ vortex lines. The critical velocity v_c after the jump is changed and is generally smaller than before. The subsequent deceleration to the annihilation threshold in Fig. 1(b) shows that v_c is reduced from 1.2 mm/s to 0.26 mm/s. Obviously, this behavior is caused by a transition from one texture to another. The vortex bursts ($\circ$ in Fig. 2) take place only at high temperatures $T \gtrsim 0.7\, T_c$. This is consistent with the fact that the

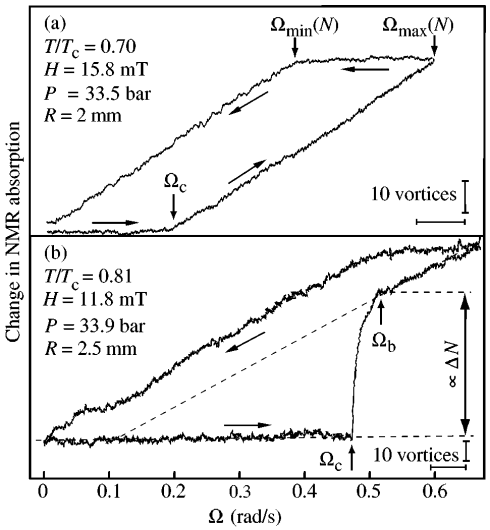

FIG. 1. NMR absorption at the vortex satellite peak during a slow acceleration/deceleration cycle: (a) regular vortex formation at approximately constant v_c and (b) burstlike vortex formation followed by the regular process. The dashed line shows the extrapolation to $N \longrightarrow 0$ in the final state where the regular process has set in with a reduced v_c.

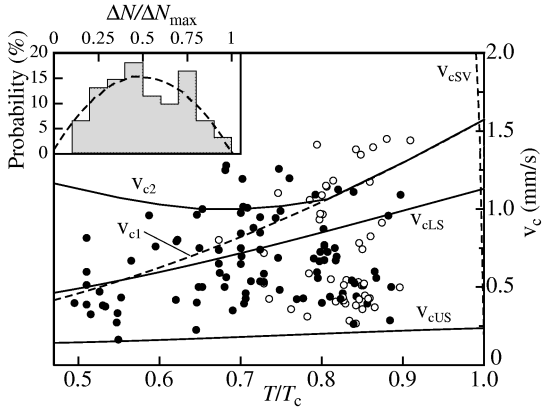

FIG. 2. Critical velocities as a function of the temperature T in axial field ($H = 9.9 - 15.8$ mT, pressures $29.3 - 34.2$ bar). The experimental results, which represent a variety of sample histories, are classified as regular ($\bullet$) and burstlike ($\circ$) vortex formation. The solid lines denote instabilities towards vortex formation in different one-dimensional textures: v_{c2} of uniform or helical texture, v_{cLS} of locked soliton texture, and v_{cUS} of an unlocked soliton. The dashed lines show the phase boundary between uniform and helical textures v_{c1}, and the instability to singular vortices v_{cSV} (estimated from Ref. [15]). Inset: Distribution of the number of vortices ΔN in a burst, normalized to the maximum possible increase $\Delta N_{max} = (2\pi R^2/\kappa)(\Omega_b - 0.16\sqrt{\Omega_b}) - N_i$, where N_i is the initial vortex number and Ω_b is defined in Fig. 1.

energy barriers between different textures are smaller at higher temperatures.

Curve v_{c2} in Fig. 2 is a theoretical result for the vortex instability of an initially uniform texture. It roughly agrees with the largest measured v_c's. Some measured values are larger than the theoretical upper limit, which may arise from inaccurate parameter values in the calculation (see below). In order to justify theoretically the texture dependence of v_c, we have calculated two simple cases of initially inhomogeneous texture. A locked soliton (LS) is a planar object where both $\hat{\mathbf{d}}$ and $\hat{\mathbf{l}}$ turn from parallel to $\mathbf{v}$ on one side to antiparallel to $\mathbf{v}$ on the other side of the wall, while they are locked to each other ($\hat{\mathbf{d}} \equiv \hat{\mathbf{l}}$). Such a texture becomes unstable against vortex formation at the velocity v_{cLS}. Another type of domain wall is an unlocked soliton (US), where $\hat{\mathbf{d}} = \hat{\mathbf{l}}$ on one side and $\hat{\mathbf{d}} = -\hat{\mathbf{l}}$ on the other. When its plane is perpendicular to $\mathbf{v}$, vortices are created at the velocity v_{cUS} [17]. These simple cases span the spread of the measured v_c in Fig. 2. This makes it plausible that the three-dimensional texture and its defects in the cylinder are responsible for all of the variation in v_c.

The data in Fig. 2 have been collected under a variety of prehistories of sample preparation. We now demonstrate that more reproducible results are obtained if the initial state is prepared using a procedure which favors an equilibrium texture. Experimentally, textural metastability is best avoided by cooling slowly ($dT/dt \sim -1\ \mu$K/min) through T_c at nonzero Ω. For consistent v_c values, Ω must not be reduced to zero at any point during the v_c measurements. The critical velocities measured under these conditions are shown in Fig. 3 in axial ($\bullet, \blacksquare$) and in transverse field ($\circ, \square$).

Insets (a) and (b) in Fig. 3 display two candidates for the $\hat{\mathbf{l}}$ texture in a rotating cylinder in axial field. The "circular" texture (a) is symmetric in rotations around the cylinder axis but the "double half" (b) has only reflection symmetry. In both textures the boundary condition fixes $\hat{\mathbf{l}}$ perpendicular to the wall but the counterflow bends it azimuthal already at distances $\sim\xi_d$. Concerning the flow properties, the circular texture is equivalent to the uniform texture, and thus vortices are here expected to be created at v_{c2}. In contrast, the double-half texture contains two locked solitons, which means that vortices are created already at v_{cLS}. The fact that the measured v_c data in Fig. 3 lies consistently above v_{cLS} suggests that the circular texture is created in cooling through T_c in rotation. Thus the measurement of v_c gives information about textures which is difficult to get by other techniques [18].

In transverse field the texture depicted in inset (c) is expected. The flow is here parallel to the field in two sectors of the cylinder. There it becomes unstable toward vortex formation at $v_{c\parallel} = v_d\rho_\parallel/\sqrt{\rho_\perp(\rho_\perp - \rho_\parallel)}$, as calculated by Fetter [10]. The measured data ($\circ$, $\square$, $\triangle$) agree with this prediction.

Figure 3 also displays v_c measurements ($\times$) in the presence of an unlocked soliton, whose plane is perpendicular to Ω. It is identified from a characteristic satellite peak in the NMR spectrum [19]. Also this object seems to reduce v_c to a low but well defined value.

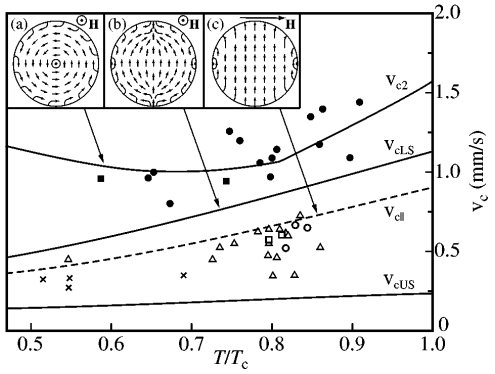

FIG. 3. Critical velocities in selected cases. (i) We cool slowly through T_c under rotation. In axial field this gives results ($\bullet, \blacksquare$) near the instability limit v_{c2} of the circular texture (inset a). In transverse field the corresponding results ($\circ, \square$) are near the instability limit $v_{c\parallel}$ [10] of the expected texture (inset c). There is no crucial difference if the magnetic field H is on during cooling ($\blacksquare, \square$) or it is switched on later ($\bullet, \circ$). The scatter in the data [which exceeds that of v_c in Fig. 1(a)] indicates that the control over the texture is limited, possibly due to the end plates of the cylinder. (ii) In transverse field v_c seems to be less sensitive to the texture, as shown by data ($\triangle$) with varied prehistories. (iii) Often a transverse soliton plane ($\perp\Omega$) is formed when cooling rapidly through T_c at $\Omega = 0$. In these cases a low v_c is found ($\times$, in axial field).

The measurements of v_c can also be carried out as a function of the magnetic field. The procedure is to accelerate in the desired field, after which the field is changed to the NMR value at constant Ω, and then v_c is determined by decelerating to the annihilation threshold (Ω_{min} in Fig. 1). The method works if $v_c(H)$ does not increase with decreasing H. Indeed, we find (axial field, 33.9 bar, $T/T_c = 0.75 - 0.85$) that v_c starts to decrease below about 3 mT, but remains finite down to zero field: $v_c(H = 0) = 0.2 - 0.6$ mm/s. This is somewhat lower than deduced by Saundry *et al.* from their measured critical flow rate at temperatures $T/T_c > 0.9$ [13].

Calculations.—The critical velocities were calculated assuming that the order parameter depends only on one coordinate x. The energy functional (1) was minimized numerically for different values of the drive velocity v_n. The values of the parameters are from Ref. [19], except that we use g_d determined from the NMR shift in the B phase, corrected by trivial strong-coupling effects. No adjustable parameters are contained in the calculations.

For helical textures the minimization gives the energy $F(v_n, q)$, where q is the fundamental wave vector of the helix. Although the periodic boundary conditions in the rotating container tend to fix q, our simulation of the dynamics gives transitions from one value of q to another. As a consequence, q approximates $q_0(v_n)$, which corresponds to the minimum of $F(v_n, q)$. [For stability both the eigenvalues of the second derivative matrix of $F(v_n, q)$ have to be positive.] At v_{c2} the opening angle $\beta(x)$ locally starts to grow larger than $\beta \lesssim 60°$ found for stable helices and eventually sweeps through 180°. Previously, v_{c1} and an estimate of v_{c2} have been calculated near T_c by Lin-Liu *et al.* [8]. We find that in high field (Fig. 2) the helical texture is not stable above $0.8\,T_c$, but at lower temperatures v_{c2} grows considerably above v_{c1}.

In low fields ($\lesssim H_d$) v_{c1} drops and vanishes at $H = 0$ when $T < 0.85\,T_c$, while v_{c2} is nearly independent of H. The observed reduction of the measured v_c probably arises because the texture at small H becomes more susceptible to different perturbations such as heat flows or end plates of the cylinder.

In the presence of solitons, the precession of the whole soliton texture around x leads to phase slippage. In zero field, both v_{cLS} and v_{cUS} vanish because there is nothing to resist the precession. Such precessing states of both the LS and the US have been studied in Refs. [20,21]. In contrast, a field $\mathbf{H}$ perpendicular to x gives rise to a finite v_c, as calculated approximately for the US by Vollhardt and Maki [5,22]. We find a much lower v_{cUS} than reported previously.

In conclusion, our measurements of vortex formation in ^{3}He-*A* are the first to allow detailed comparison with theoretical calculations. The quantitative agreement is much better than found for v_c in other superfluids (^{4}He-II and ^{3}He-B). We find that the critical velocity depends on the bulk $\hat{\mathbf{l}}(\mathbf{r})$ texture. The maximal critical velocity we associate with the equilibrium texture in axial field, while the minimal velocity is a characteristic of textures incorporating unlocked solitons.

We thank R. Hänninen and J. Ruohio for valuable help. This work is funded by the EU Human Capital and Mobility Program (No. CHGECT94-0069).

[1] R. J. Donnelly, *Quantized Vortices in He-II* (Cambridge Univ. Press, Cambridge, 1991).
[2] *Nucleation*, edited by A. C. Zettlemoyer (Marcel Dekker, New York, 1969).
[3] P. W. Anderson, Rev. Mod. Phys. **38**, 298 (1966).
[4] P. Bhattacharyya, T.-L. Ho, and N. D. Mermin, Phys. Rev. Lett. **39**, 1290 (1977).
[5] D. Vollhardt, and P. Wölfle, *The Superfluid Phases of Helium 3* (Taylor & Francis, London, 1990).
[6] Ü. Parts *et al.*, Europhys. Lett. **31**, 449 (1995).
[7] D. Vollhardt, Y. R. Lin-Liu, and K. Maki, J. Low Temp. Phys. **37**, 627 (1979).
[8] Y. R. Lin-Liu, D. Vollhardt, and K. Maki, Phys. Rev. B **20**, 159 (1979).
[9] A. L. Fetter and M. R. Williams, Phys. Rev. B **23**, 2186 (1981).
[10] A. L. Fetter, Phys. Rev. B **24**, 1181 (1981).
[11] M. A. Paalanen and D. D. Osheroff, Phys. Rev. Lett. **45**, 362 (1980).
[12] H. M. Bozler, in *Helium Three*, edited by W. P. Halperin and L. P. Pitaevskii (North-Holland, Amsterdam, 1990), p. 695.
[13] P. D. Saundry, M. R. Thoman, L. J. Friedman, C. M. Gould, and H. M. Bozler, J. Low Temp. Phys. **86**, 401 (1992).
[14] The vortices under these conditions are of "continuous unlocked" type with $\kappa = 2(h/2m)$ [15].
[15] Ü. Parts *et al.*, Phys. Rev. Lett. **75**, 3320 (1995).
[16] $\Omega_{min}(N)$ does not coincide exactly with $\Omega_v(N)$, where $v = 0$, but the two are separated by small counterflow amounting to $\Omega_v = \Omega_{min} - 0.16\sqrt{\Omega_{min}}$ (in rad/s); see V. M. Ruutu *et al.*, Czech. J. Phys. **46**, 9 (1996).
[17] Strictly taken, v_{cUS} is the theoretical critical velocity for the initial growth of a vortex sheet (measured in Ref. [19]) rather than for the nucleation of vortex lines.
[18] Rotating textures in a slab geometry have also been identified in recent mutual friction measurements: A. J. Manninen, T. D. Bevan, J. B. Cook, H. Alles, J. R. Hook, and H. E. Hall, Phys. Rev. Lett. **77**, 5086 (1996).
[19] Ü. Parts *et al.*, Physica (Amsterdam) **210B**, 311 (1995).
[20] J. R. Hook and H. E. Hall, J. Phys. C **12**, 783 (1979).
[21] R. C. Dow and J. R. Hook, Phys. Rev. Lett. **55**, 2305 (1985).
[22] D. Vollhardt and K. Maki, Phys. Rev. B **20**, 963 (1979); **23**, 1989(E) (1981) .